Eur. Phys. J. B **55**, 347–354 (2007)
DOI: 10.1140/epjb/e2007-00078-6

THE EUROPEAN PHYSICAL JOURNAL B

Frictional stick-slip dynamics in a nonsinusoidal Remoissenet-Peyrard potential

G. Djuidjé Kenmoé[a] and T.C. Kofané[b]

Département de Physique, Laboratoire de Mécanique, Faculté des Sciences, Université de Yaoundé I, B.P. 812 Yaoundé, Cameroun

Received 10 July 2006 / Received in final form 18 December 2006
Published online 22 March 2007 –

Abstract. Frictional stick-slip dynamics is studied theoretically and numerically in a model of one oscillator interacting with a nonsinosoidal subtracted potential. We focus our attention on a class of parameterised one-site Remoisenet-Peyrard potential $U_{RP}(X,r)$, whose shape can be varied as a function of parameter r and which has the sine-Gordon shape as the particular case. The dynamics of the model is carefully studied, both numerically and analytically. Our numerical investigation, which involves bifurcation diagrams, shows a rich spectrum of dynamical behavior including periodic, quasi-periodic and chaotic states. On the other hand, and for a good selection of the parameter systems, the motion of the particle involves periodic stick-slip, erratic and intermittent motions, characterized by force fluctuations, and sliding. This study suggests that the transition between each of motion strongly depends on the shape parameter r. However, the stick-slip phenomena can be observed for all values of the shape parameter r in the range $|r| < 1$. The analytical analysis of the dry friction reveals that the dynamic depends non trivially on the shape parameter r, which shows the importance of deformable substrate potential in the description of real physical systems.

PACS. 46.55.+d Tribology and mechanical contacts – 68.35.Iv Acoustical properties – 81.40.Pq Friction, lubrication, and wear

1 Introduction

The interest in elucidating dissipative processes [1,2] on various spatial and temporal scales, from microscopic to macroscopic, that may occurs in all machines and mechanism is justified by modern experimental technologies that have made it possible to study wearless friction between clean and atomically flat surface [3,4]. In particular, much attention has been recently developed within the field of nanotribology in the understanding of the nature of friction at the microscopic scale [1–4] sheared liquids confined between two atomically smooth solid surfaces provide a good example of a system where a broad range of phenomena and different behaviors have been experimentally observed. The majority of surface force apparatus (SFA) measurements have been performed with atomically flat mica surface [5–9]. On the other hand, great attention is paid to the dynamics of dry friction, that is, velocity independent friction. Moreover, it is now well understood that the dynamic behavior in several fields of science with dry friction is nonlinear because Coulomb's laws [1] make a distinction between static friction force and kinetic friction force. The static friction force is the force necessary to start sliding or a constraining force during sticking (stick regime) while the kinetic friction force is the force necessary to keep sliding at a constant velocity (slip regime). If the static friction force is larger than the kinetic one, or that the kinetic friction force drops rapidly at small speeds, the sliding surfaces alternately switch between sticking and slipping in a more regular or irregular fashion. This unstable motion is repeated in rapid succession until the slide reaches a certain velocity called the critical velocity [10]. The results of these studies are very encouraging, but in those systems, the shape of the nonlinear one-site potential may deviate considerably from that attributed to the local potential. Thus, the classical systems, which are generally associated with rigid potentials, as sine-Gordon, cannot be satisfactorily used to describe them. Introduction of deformable potentials in the description of those systems [11] is therefore indispensable to obtain general results that can be applied to them. Considerable effort has been made in the last two decades to use deformable potentials in the context of the solitary waves [12–16], and recently in the chaotic system [17–20]. In spite of these efforts, little is known about stick-slip phenomena, which involve deformable potentials. Therefore, the present work is a contribution to the growing field of the concept of friction, and the problem of stick-slip

[a] e-mail: kdjuidje@yahoo.fr
[b] e-mail: tckofane@yahoo.com

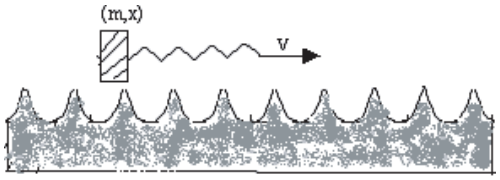

Fig. 1. Schematic sketch of model geometric.

motion in a more complex periodic nonsinusoidal potential, which is of interest to our present investigation, in which the shape parameter could account for the temperature or pressure dependence, or the geometry of the surface of the metallic surface.

The paper is organized as follows. In Section 2, we define the model and present the equation of the field displacement. Our analysis starts in Section 3 by the numerical investigations including computation of bifurcations diagrams. The properties of the pure dry friction force, defined as the dissipated energy per unit length are carried out in Section 4. Finally, in Section 5 the main contributions of the paper are summarized.

2 Dynamical treatment

2.1 Model description and Lagrangian formalism

The purpose of this subsection is to introduce our model schematised in Figure 1. It includes a particle of mass m which moves along a straight line. The particle is pulled by a spring with force constant K. This spring is connected to a stage moving with a constant velocity V, and the displacement of the particle is characterized by the variable X. To model the interaction between the straight line and the particle, we consider a general class of nonsinusoidal oscillators like the Remoissenet-Peyrard (RP)-potential [12,13] which is one of the most popular of the deformable potentials. This potential,

$$U_{RP}(X,r) = U_0(1-r)^2 \frac{1-\cos(2\pi X/b)}{1+r^2+2r\cos(2\pi X/b)} \qquad |r|<1 \quad (1)$$

has constant amplitude and is 2π-periodic in X, where X denotes the displacement field; U_0 is a constant which measures the amplitude of the potential (1), while b is the period of the potential. The shape of the potential is defined by the parameter r. For $r>0$, the nonsinusoidal RP potential has flat bottoms separated by thin barriers (see Fig. 2a, for $r=0.6$), while for $r<0$, it has the shape of sharp wells separated by flat wide barriers (see Fig. 2b, for $r=-0.6$). For $r=0$, the nonsinusoidal RP potential (1) reduces to the sinusoidal potential which is the familiar sine-Gordon (sG) potential. From the Lagrangian for the nonconservative systems, the equation of motion for the particle can be written in dimensionless form as:

$$\ddot{x} + \alpha\dot{x} + c(1-r^2)^2 \frac{\sin x}{(1+r^2+2r\cos x)^2} + (x - v\tau) = 0 \quad (2)$$

where $x = 2\pi X/b$, is the coordinate of the particle, in units of the period of the potential b, $\tau = \Omega t$ is the dimensionless time, $\Omega = \sqrt{K/m}$ the frequency of the free oscillations of the particle, $\alpha = \mu/(m\Omega)$, is the dimensionless constant friction which account for dissipation due to phonons and/or others oscillations, and $v = V/(b\Omega)$ is the dimensionless velocity, $c = 4\pi^2 U_0/Kb^2$ is a dimensionless measure of the strength of the periodic potential compared to that of the spring. Equation (2) can describe a dissipative parametrically driven pendulum, in a nonsinusoidal subtracted potential. Below, we discuss the dependence of the motion of the particle on the parameters of the system. The main objective is to deduce information on the microscopic properties of the system from the observed dynamics of the particle. For this purpose, one needs to understand the dependence of the dynamics on the mechanical (external) parameters and the parameters of the embedded system (internal).

2.2 Numerical analysis of the motion of the particle

The present subsection presents the results of the numerical treatment. In order to understand dynamical processes of the particle, equation (2) has been integrated numerically with fourth-order Runge-Kutta scheme with the time step equals 0.055 and the initial conditions $\dot{x}(0) = x(0) = 0$. Depending on the parameters of the system, the present model can present regular or chaotic behaviors. Thus, in a particular set of the parameters of the system, and increasing the velocity v, the behavior of the particle presents: stick-slip, intermittent and sliding motions. The transition between the stick-slip and intermittent motions is above a critical velocity $v_c^{(1)}$, while $v_c^{(2)}$ corresponds to the transition between intermittent and sliding motions. These two critical velocities strongly depend on the physical parameters of our model, and particularly on the shape parameter r.

2.2.1 Phase space and stroboscopic observation

To present the dynamical behavior of the particle, we use the phase space representation of the expression $z = x - v\tau + \alpha v$ versus $\dot{z}$. With the variation of the parameters c, and v, the numerical results are shown in Figures 3a–3c, where one can see, a periodic structure or limit cycle with period 1 (see Fig. 3a), where the curve is obtained for the set of parameters $c=5$, $\alpha=0.5$, $v=3$ and $r=-0.5$. Moreover, with the following parameters $c=5$, $\alpha=0.5$, $v=1$ and $r=0.2$, we obtain a limit cycle with period 2 (see Fig. 3b). Taking the parameter $c=5$, $\alpha=0.5$, $v=1$ and $r=-0.5$, we obtain

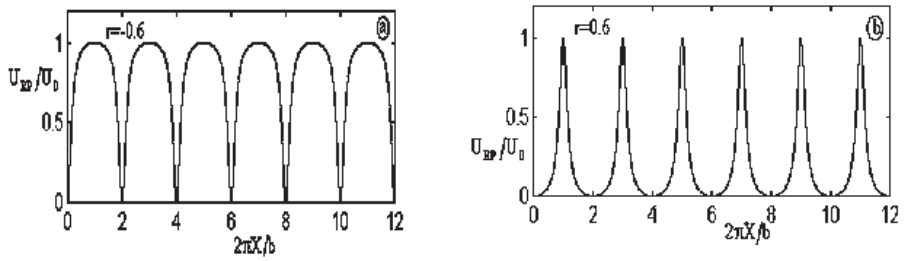

Fig. 2. Form of RP potential for (a): $r = -0.6$, (b): $r = 0.6$.

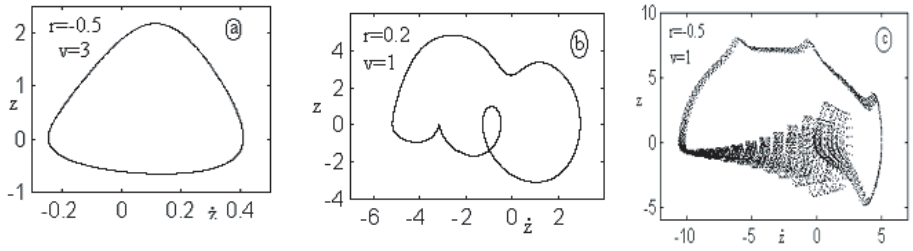

Fig. 3. Phase space representation of the motion of the particle for selected values of the parameters v and r, with $c = 5$ and $\alpha = 0.5$. (a) Limit cycle for $r = -0.5$ and $v = 3$; (b) period 2 for $r = 0.2$ and $v = 1$; (c) chaotic behavior for $r = -0.5$ and $v = 1$.

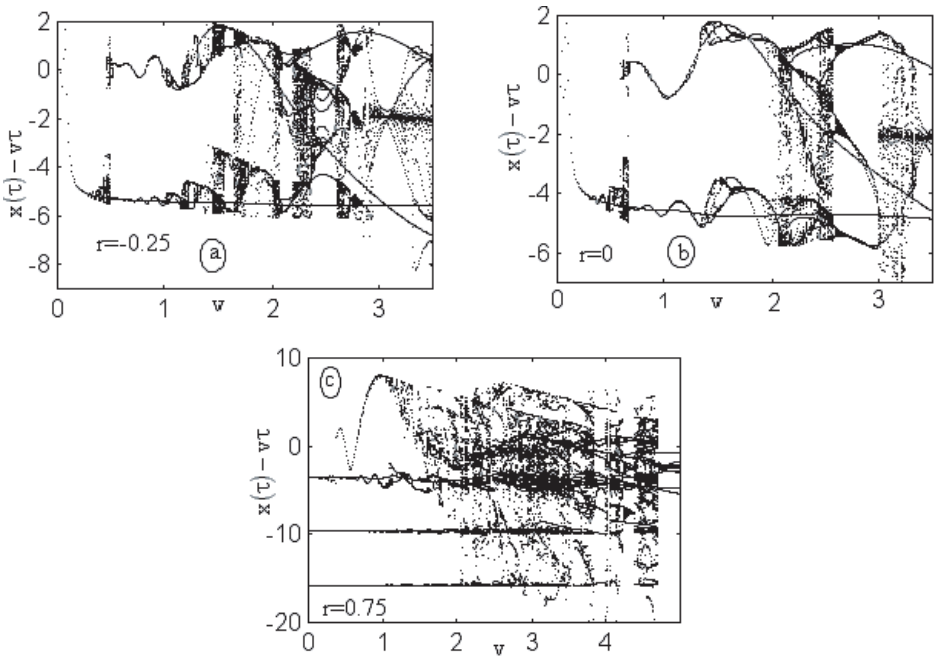

Fig. 4. Stroboscopic representation plot $x(\tau) - v\tau$ at time $\tau = 2\pi n/v$ for $n = 1, 2, ..., 100$ versus v, for three selected values of parameters r indicated in the graph; with $c = 5$ and $\alpha = 0.5$.

a chaotic structure (see Fig. 3c). Furthermore, numerical solutions show that for a given damping coefficient α, and after a time $\tau \gg 2\pi/v$, the function $x(\tau) - v\tau$ usually becomes periodic with period $2\pi n/v$ (n integer) and $x\Big(\tau + (2\pi n/v)\Big) = x(\tau) + 2\pi n$ where the integer n depends on of the parameters c, and r, and also on the initial conditions. For the parameters $c = 4$, $\alpha = 0.5$ and for $n = 1, 2, 3, ..., 100$, Figures 4a–4c and 5a–5c display the value of $x(\tau) - v\tau$ for integer multiples of periods. One can see in Figures 4a–4c, the stroboscopic representation as a function of v for three values of the shape parameter r. While Figures 5a, 5b show the stroboscopic representation as a function of the shape parameter r for certain values of the velocity v. In the range $-0.5 < r < 0.5$, the system is regular at the low velocity. This regular behavior disappears with increasing velocity v. These stroboscopic representations display bifurcation and chaotic motions, and show the range of velocity v or parameters k_0 where the motion is chaotic or regular. As we will see below, for

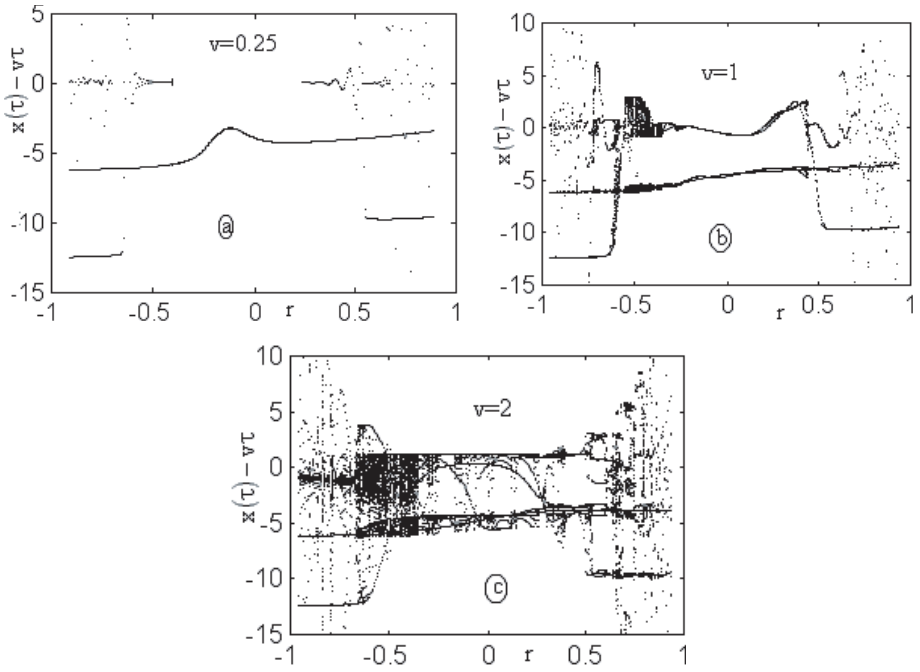

Fig. 5. Stroboscopic representation plot $x(\tau) - v\tau$ at time $\tau = 2\pi n/v$ for $n = 1, 2, ..., 100$ versus r, for three selected values of velocity v indicated in the graph; with $c = 5$ and $\alpha = 0.5$.

the other set of the system parameters, the model under consideration exhibits stick-slip phenomena.

2.2.2 Stick-slip phenomena

The stick-slip motion is characterized by two regimes: in the first regime, the particle is trapped (creep) by the subtract and make microscopic oscillations in the minima of the potential

$$U(X, r, t) = U_{RP}(X, r) + \frac{1}{2}K(X - Vt). \tag{3}$$

Figures 6a, 6b show the form of this potential for two selected values of the shape parameter r. Then, a rapid sliding motion takes place and moves the particle in the next minima of the potential. Figure 7a, in the phase portrait $(x, \dot{x})$, presents the typical phenomena of stick-slip motion. In this figure, one can then observe positions where the particle is trapped by the substrate and makes microscopic oscillations, stops an instant when its velocity $\dot{x}$ becomes zero. This velocity $\dot{x}$ which is zero, increases suddenly, the particle slides rapidly and goes in the next minima of the potential; and the same scenario begins. One can observe that the particle goes on one minimum to another in a rapid and regular way, i.e. in a periodic way. Moreover, the form of oscillations, which is present in Figure 7b, is the same in each well of the potential and this characterizes the periodic stick-slip motion. Note that this form of oscillations strongly depends on the parameters of our physical system. As shown in Figure 7b, one can observe the interval [a,b] which corresponds to a very slow motion (creep) of the particle located in the minima of the potential. The particle starts to slide at the saddle point b, where the instability occurs, approaches the maximal velocity at the point c, and comes again to rest at the point a, but in the next minima of the potential. At the point of instability b, the spring force reaches a maximum value corresponding to the static friction force f_s (see Fig. 9a). The static friction force equals the maximum value of the force acting on the particle; this force, depend explicitly on the shape parameter r as follows

$$f_s = 2\pi c \left(\frac{1 - r^2}{1 + r^2}\right)^2. \tag{4}$$

Figure 8 shows the variation of the static friction as a function of r. One can easily see the symmetric property as a function of r. During the sliding, the spring force $f_r = -(x - v\tau)$ decreases until it reaches a value f_k, where the sliding ceases and the particle is trapped again at a potential minimum. The evolution of the spring force is plotted in Figures 9a–9c in three regimes of the particle motion corresponding to the stick-slip, intermittent and smooth sliding motions, respectively. This evolution permits us to detect the critical velocities $v_c^{(1)}(r)$ and $v_c^{(2)}(r)$.

2.2.3 Influence of the shape parameter r on the transition from stick-slip motion to modulated sliding state

As the stage velocity increases, the stick-slip motion of the particle becomes more erratic and intermittent, and then changes to periodically modulated sliding state. Figure 10 shows the dynamical phase diagram (in the $r - v$ plane), which presents regions of the shape parameter r that correspond to different regimes of the motion of the

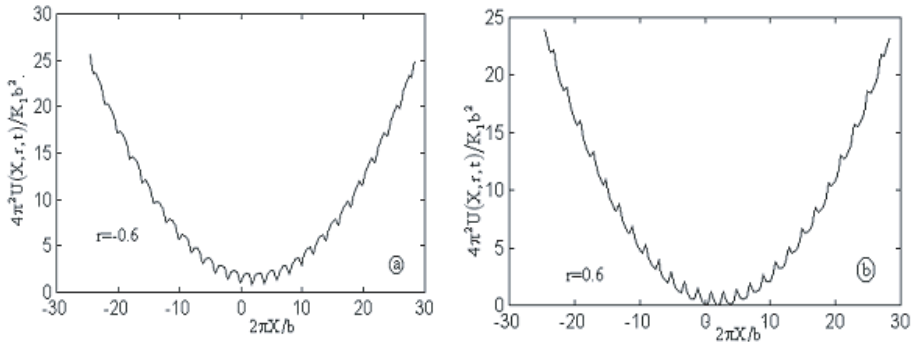

Fig. 6. Dimensionless total potential $4\pi^2 U(X, r, t/Kb^2)$ versus the dimensionless particle coordinate $2\pi X/b$, drawn for $c = 5$ and $\alpha = 4$, (a) $r = -0.6$; (b) $r = 0.6$.

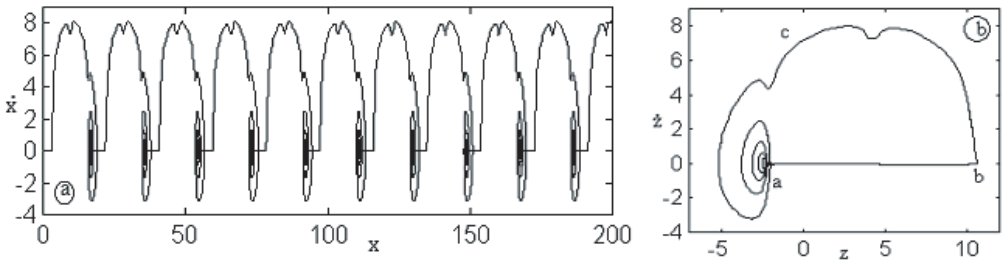

Fig. 7. With the set of parameters $c = 4$, $r = 0.6$, $\alpha = 0.4$ and $v = 0.06$. (a) Displacement of the particle in the stick-slip regime; (b) form of oscillations in the minima of the potential.

particle. Stick-slip motion and smooth sliding occur respectively to the left at the line $v_c^{(1)}(r)$ and to the right of the line $v_c^{(2)}(r)$. The system exhibits an intermittent motion in the range of parameters between these two curves. The lines $v_c^{(1)}(r)$ and $v_c^{(2)}(r)$ describe the r dependence of the critical velocities corresponding to transitions between different states of motion. These critical velocities have been found by numerical analysis of the solutions of equation (2). As the driving velocity varies from $v_c^{(1)}(r)$ to $v_c^{(2)}(r)$, the motion of the particle bifurcates from the periodic stick-slip motion to modulated sliding state. Above $v_c^{(1)}(r)$, the stick-slip motion becomes erratic and intermittent. For a wide range of the system parameters, we find that the motion is chaotic (see Fig. 9b). In this figure it appears that the transition from the periodic stick-slip motion to smooth sliding which occurs in high velocity also depends on the shape parameter r.

3 Pure dry friction

We consider very small velocities $v \ll 1$, but consider times, which are larger so that $Vt \to L_0$ is finite. In this case, the stage is effectively at rest during the fall of the particle into a minimum potential. At all times, except during the fall, the particle is in a minima of the total potential $U(X, r, t)$. One of the key parameter used to characterize the beginning of the drop is the second derivative $d^2U(X, r, t)/dX^2$, which changes sign when an instability occurs. After a dropping motion, the particle

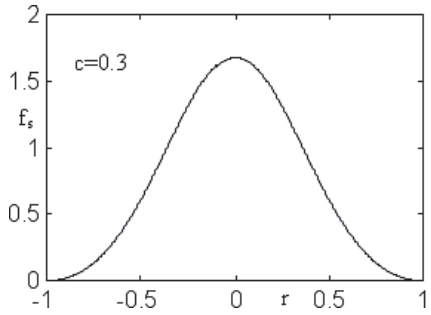

Fig. 8. Evolution of the static friction force as a function of the shape parameter r for $c = 0.3$.

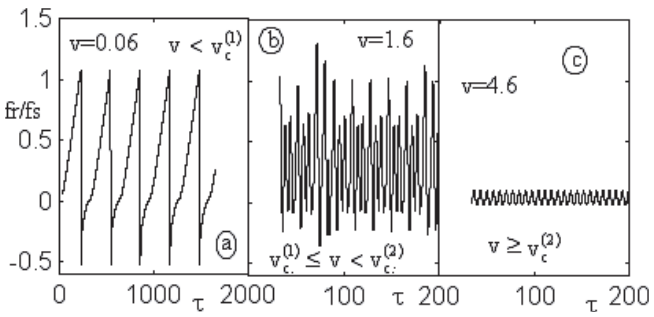

Fig. 9. Time series of the spring force corresponding to the three regimes of the particle motion: (a) stick-slip regime, for $v = 0.06$; (b) intermittent regime, for $v = 1.6$; (c) sliding for $v = 4.6$. Parameters are the same as in Figures 3, 6, except for the velocities.

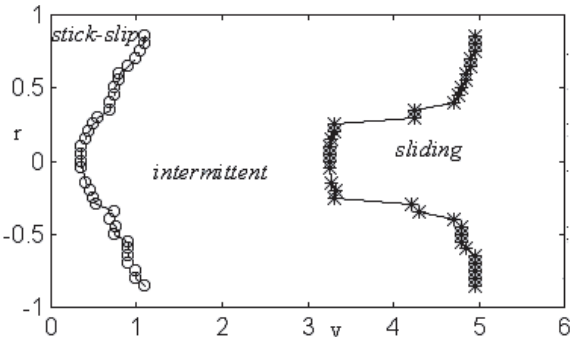

Fig. 10. Dynamical phase diagram for the motion of the particle for $c = 4$, $\alpha = 0.4$. The first curve $v_c^{(1)}(r)$ indicates the boundary between the stick-slip and intermittent motions, and the second curve $v_c^{(2)}(r)$ is the velocity boundary of the sliding motion. Open circles and stars show the results of numerical calculations of $v_c^{(1)}(r)$ and $v_c^{(1)}(r)$, respectively.

is still at a minimum potential. When there are several minima of $U(X, r, t)$, the question of where it comes to rest can only be solved using the equation of the motion. The position L_0 and X_0 of the stage and the particle at the beginning of the drop, respectively, are now determined at the saddle point given by

$$\frac{dU(X,r,t)}{dX} = 0 \tag{5a}$$

$$\frac{d^2U(X,r,t)}{dX^2} = 0. \tag{5b}$$

Such a scheme is expected to be valid if we assume that the viscous friction is sufficiently large so that the particle comes at rest in the next minimum. The energy dissipated during the drop is

$$\triangle W = U(X_0, L_0) - U(X_1, L_0). \tag{6}$$

Parameters X_0, L_0 and $U(X_0, r, L_0)$ can be evaluated analytically. $U(X_1, r, L_0)$ is evaluated numerically, where X_1 is the next larger value of X that satisfies equation (5a). In addition, the notations

$$x_0 = \frac{2\pi X_0}{b}, \qquad x_1 = \frac{2\pi X_1}{b}, \qquad l_0 = \frac{2\pi L_0}{b} \tag{7}$$

are introduced in dimensionless form. In this sense, x_0 is the solution of the cubic equation

$$a_3 \cos x^3 + a_2 \cos x^2 + a_1 \cos x + a_0 = 0 \tag{8}$$

where the coefficients $a_i (i = 1, 2, 3)$ depend on the shape parameter as

$$\begin{aligned} a_3 &= 8r^3 \\ a_2 &= 12r^2(1 + r^2) - 2cr(1 - r^2)^2 \\ a_1 &= c(1 - r^2)^2(1 + r^2) + 6r(1 + r^2)^2 \\ a_0 &= (1 + r^2)^3 + 4cr(1 - r^2)^2. \end{aligned} \tag{9}$$

To obtain the solution of equation (8), it is useful to introduce the transformations

$$\alpha = \frac{a_2}{a_3}, \quad \beta = \frac{a_1}{a_3}, \quad \gamma = \frac{a_0}{a_3}. \tag{10}$$

Applying the transformation of Thirnaus gives all solutions of equation (8) as follows

$$\begin{aligned} x_0 &= \arccos\left(\sqrt{\frac{-4}{3p^3}}\cos\left(\frac{\theta}{3} + \frac{2k\pi}{3}\right) - \frac{\alpha}{3}\right), \\ \theta &= \frac{1}{3}\arccos\left(q\sqrt{\frac{-27}{4p^3}}\right), \quad k = 0, 1, 2 \end{aligned} \tag{11}$$

with

$$p = \beta - \frac{\alpha^2}{3} \quad \text{and} \quad q = -\frac{\alpha}{27}(2\alpha^2 - 9\beta) + \gamma \tag{12}$$

and

$$l_0 = x_0 + c(1 - r^2)^2 \frac{\sin x_0}{(1 + r^2 + 2r\cos x_0)^2}. \tag{13}$$

In the calculation, the condition $p < 0$ is needed for any value of the shape parameter r.

With the value of l_0, we look for the next value $x = x_1$, which satisfies equation (5.a), that is

$$x_1 + c(1 - r^2)^2 \frac{\sin x_1}{(1 + r^2 + 2r\cos x_1)^2} = l_0. \tag{14}$$

The dry friction force F is defined as the dissipated energy per unit length, that is $F = \Delta W/b$, which in dimensionless form is, $f = F/(Kb/4\pi^2)$. This dry friction force f is given by

$$\begin{aligned} f(c) = {} & \frac{1}{2}(x_0 - l_0)^2 + c(1 - r)^2 \frac{1 - \cos x_0}{1 + r^2 + 2r\cos x_0} \\ & - \frac{1}{2}(x_1 - l_0)^2 - c(1 - r)^2 \frac{1 - \cos x_1}{1 + r^2 + 2r\cos x_1}. \end{aligned} \tag{15}$$

It appears in equation (4) that the dimensionless static force depends much on the dimensionless measure of the strength of the periodic nonsinusoidal RP-potential c and the shape parameter r. It also appears in equation (15) that the dimensionless dry friction depends on the dimensionless measure of the strength of the periodic nonsinusoidal RP potential c and the shape parameter r. Due to its analytical complexity, it has been determined only numerically through the variable c (with all the information about the function determined in the range $10^{-2} < (c - 1) < 10^4$ in the log-log plotting). Further, from Figures 11a–11c, it should be noted that these two forces present a symmetric behavior as a function of the shape parameter r.

In the particular case where $r = 0$, the average friction force can be calculated analytically for two limiting cases [21]

$$\begin{aligned} f = {} & \frac{9}{2}(c - 1)^2 - \frac{18}{5}(c - 1)^3 + \frac{531}{175}(c - 1)^4 \\ & + \bigcirc((c - 1)^5) \quad \text{for} \quad c - 1 \ll 1 \end{aligned} \tag{16}$$

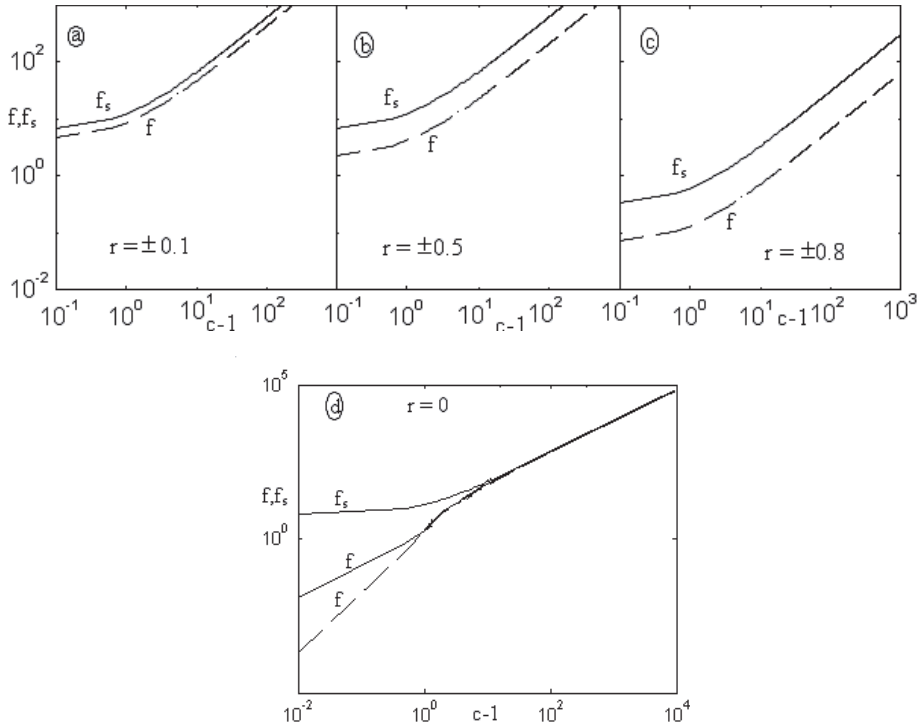

Fig. 11. Dimensionless dry friction force as a function of $c-1$ for arbitrary slow motion ($v \to 0$), for selected values of the shape parameter r indicated on the graphs. The parameter c is the dimensionless measure of the amplitude of the potential. Dashed line is obtained by the approximated analytical estimates.

and

$$f = 2\pi c - 2\pi^2 + \frac{8}{3}\pi^{3/2}c^{-1/2} - \pi c^{-1} + \bigcirc((c)^{-3/2}) \text{ for } c \gg 1. \tag{17}$$

The corresponding static frictional force here is $f_s = 2\pi c$ ($r = 0$). In this case, it is interesting to compare numerical results of this force with the approximated estimates (Eqs. (16, 17)). Thus, we carry out a direct numerical evaluation of dry friction force (Eq. (15)) with $a_3 = a_2 = 0$, $a_1 = c$ and $a_0 = 1$. This allows us to obtain $x_0 = \arccos(-1/c)$, $l_0 = \arccos(-1/c) + \sqrt{c^2 - 1}$ and x_1 is evaluated numerically with $x_1 + c \sin x_1 = l_0$. Plotting in the same graph, the approximated (dashed line) dry friction force and the exact one (solid line), the comparison can easily be done. For these calculations, we have been able to reproduce in the range $(c-1) > 1$ as indicated in Figure 11d, the exact result in good agreement with approximation that we have considered.

4 Conclusion

In this work, we have been able to describe dynamic stick-slip friction in a non linear model that contains a periodic nonsinusoidal substrate potential. The nonlinearity of the problem gives rise to a variety of complex features, such as bifurcation, chaotic motion, periodic stick-slip, erratic and intermittent motions, characterized by force fluctuations, and sliding above the critical velocity $v_c^{(2)}(r)$. Intensive investigations have been carried out on equations (2) and particular attention is allocated to investigations on dry friction which depends on the parameter r. We have also shown the substantial impact of the shape parameter on static and dry frictions. These forces have a symmetric behavior as a function of the parameter r. It should be noted that the critical velocities, which present the transition between the different regimes of the particle motion, strongly depend on the shape parameter r. Our calculation also demonstrated that a variation of the shape parameter affects the dynamical phase diagram [leading to a shift of the boundary lines $v_c^{(1)}(r)$ and $v_c^{(2)}(r)$]. This deformable model leads to a variety of phenomena, which may contribute to a better description of the dry friction. In general, the shape variation of the potential is commonly ignored since all studies are limited to the sinusoidal potential, which is the leading term in the nonsinusoidal RP potential. As the periodic sinusoidal substrate potential is of important, our results have potentially an equally wide range of applications in physics and chemistry.

References

1. F.P. Bowden, D. Tabor, *Friction and Lubrication* (Oxford University Press, 1954)
2. *Fundamentals of Friction: Macroscopic and Microscopic Processes*, edited by I.L. Singer, H.M. Pollock (Kluwer Academic Publishers, Dordrecht, 1992)
3. B. Bhushan, J.N. Israelachvilli, U. Landman, Nature (London) **374**, 607 (1995)

4. B.N.J. Persson, *Sliding Friction: Physical Properties and Applications* (Springer, Berlin, 1998)
5. H. Yoshizawa, P. McGuiggan, J. Israelachvili, Science **259**, 1350 (1993)
6. H. Yoshizawa, Y.L. Chen, J. Israelachvili, J. Phys. Chem. **97**, 4128 (1993)
7. A.D. Berman, W.A. Ducke, J.N. Israelachvili, Langmuir **12**, 4559 (1996)
8. J.M. Georges, A. Tonck, J.L. Loubet, J. Phys. II **6**, 57 (1996)
9. J. Crassous, E. Charlaix, J.L. Loubet, Phys. Rev. Lett. **78**, 2425 (1997)
10. L.I. Daikhin, M. Urbakh, Phys. Rev. E **59**, 1921 (1999)
11. G. Djuidjé Kenmoé, A. Kenfack Jiotsa, T.C. Kofané, Physica D **191**, 31 (2004)
12. M. Remoissenet, M. Peyrard, J. Phys. C: Solid State Phys. **14**, L481 (1981)
13. M. Remoissenet, M. Peyrard, Phys. Rev. B **26**, 2856 (1982)
14. M. Remoissenet, M. Peyrard, Phys. Rev. B **29**, 3153 (1984)
15. T.C. Kofané, A.M. Dikande, Solid-State Com. **86**, 749 (1993)
16. A.M. Dikande, T.C. Kofané, Solid-State Com. **89**, 283 (1994)
17. S.B. Yamgoue, T.C. Kofané, Chaos, Solitons And Fractals **17**, 155 (2003)
18. S.B. Yamgoue, T.C. Kofané, Chaos, Soreflitons And Fractals **15**, 119 (2003)
19. L. Nana, T.C. Kofané, E. Coquet, P. Tchofo-Dinda, Chaos, Solitons and Fractals **12**, 73 (2001)
20. L. Nana, T.C. Kofané, E. Coquet, P. Tchofo-Dinda, Physica Scripta **62**, 225 (2000)
21. J.S. Helman, W. Baltensperger, J.A. Holyst, Phys. Rev. B **49**, 3831 (1994)